Washington University School of Medicine
Digital Commons@Becker

Open Access Publications

2018

Cross-sectional and longitudinal atrophy is preferentially associated with tau rather than amyloid β positron emission tomography pathology

Brian A. Gordon
Washington University School of Medicine in St. Louis

Austin McCullough
Washington University School of Medicine in St. Louis

Shruti Mishra
Washington University School of Medicine in St. Louis

Tyler M. Blazey
Washington University School of Medicine in St. Louis

Yi Su
Washington University School of Medicine in St. Louis

See next page for additional authors

Follow this and additional works at: https://digitalcommons.wustl.edu/open_access_pubs

Authors

Brian A. Gordon, Austin McCullough, Shruti Mishra, Tyler M. Blazey, Yi Su, John Christensen, Aylin Dincer, Kelley Jackson, Russ C. Hornbeck, John C. Morris, Beau M. Ances, and Tammie L.S Benzinger

Special Section: State of the Field: Advances in Neuroimaging from the 2017 Alzheimer's
Imaging Consortium

Cross-sectional and longitudinal atrophy is preferentially associated with tau rather than amyloid β positron emission tomography pathology

Brian A. Gordon[a,b,c,*,1], Austin McCullough[a,1], Shruti Mishra[a], Tyler M. Blazey[a], Yi Su[a],
John Christensen[a], Aylin Dincer[a], Kelley Jackson[a], Russ C. Hornbeck[a], John C. Morris[b,d],
Beau M. Ances[b,d], Tammie L. S. Benzinger[a,b]

[a]Mallinckrodt Institute of Radiology, Washington University, St. Louis, MO, USA
[b]Knight Alzheimer's Disease Research Center, Washington University, St. Louis, MO, USA
[c]Department of Psychological and Brain Sciences, Washington University, St. Louis, MO, USA
[d]Department of Neurology, Washington University, St. Louis, MO, USA

Abstract

Introduction: Structural magnetic resonance imaging is a marker of gray matter health and decline that is sensitive to impaired cognition and Alzheimer's disease pathology. Prior work has shown that both amyloid β (Aβ) and tau biomarkers are related to cortical thinning, but it is unclear what unique influences they have on the brain.

Methods: Aβ pathology was measured with [18F] AV-45 (florbetapir) positron emission tomography (PET) and tau was assessed with [18F] AV-1451 (flortaucipir) PET in a population of 178 older adults, of which 123 had longitudinal magnetic resonance imaging assessments (average of 5.7 years) that preceded the PET acquisitions.

Results: In cross-sectional analyses, greater tau PET pathology was associated with thinner cortices. When examined independently in longitudinal models, both Aβ and tau were associated with greater antecedent loss of gray matter. However, when examined in a combined model, levels of tau, but not Aβ, were still highly related to change in cortical thickness.

Discussion: Measures of tau PET are strongly related to gray matter atrophy and likely mediate relationships between Aβ and gray matter.

© 2018 The Authors. Published by Elsevier Inc. on behalf of the Alzheimer's Association. This is an open access article under the CC BY-NC-ND license (http://creativecommons.org/licenses/by-nc-nd/4.0/).

Keywords: Thickness; Atrophy; Tau; Amyloid; PET; Positron emission tomography; MRI

1. Introduction

One of the earliest established and most widely replicated neuroimaging findings in Alzheimer's disease (AD) is a reduction in gray matter and greater rates of longitudinal atrophy [1–5] seen with magnetic resonance imaging (MRI).

Similarly, lower baseline levels and greater gray matter atrophy have been found in participants with mild cognitive impairment [6], subjective memory complaints [7], and cognitively normal individuals with abnormal levels of amyloid β (Aβ) [4,5,8–10] relative to those without any AD pathology. In a clinical setting, structural pathological MRI measures and rates of change have prognostic value, predict conversion from mild cognitive impairment to AD [11–14], and an increased risk of later AD dementia in cognitively normal individuals [15].

While much of the focus has understandably been on the medial temporal lobes, loss of gray matter is not restricted to

---

these regions. Analyses looking at whole-brain spatial patterns see loss of gray matter prominently throughout the temporal, parietal, frontal, and occipital regions [3,4,6]. Prior work shows that such structural atrophy is related to levels of Aβ [5,10,16,17], but increased levels of Aβ may simply be a proxy for other AD-related pathologies such as neurofibrillary tangles (NFTs).

Positron emission tomography (PET) ligands that bind to NFTs [18–21] have provided a new biomarker to understand AD. Tau PET is elevated in AD [22–28] and in cognitively normal individuals with elevated Aβ pathology [23,25,29,30]. Elevated tau PET binding predicts other neurodegenerative biomarkers such as hypometabolism [31–33] and structural atrophy [34–36].

Owing to the accessibility and prevalence of structural MRI imaging, it is critical to understand the relationship between tau PET and gray matter integrity. Prior work has examined cross-sectional relationships between tau PET using AV-1451 and cortical thickness [34–37], finding that increased levels of tau PET binding were associated with thinner cortices, particularly in temporal, lateral parietal, and occipital regions. There is also initial evidence that prior longitudinal changes in structural MRI over a limited time window (~3 years) predict current levels of NFT pathology measured with PET [35]. This cross-sectional and longitudinal work reveals that there is a clear relationship between in vivo measures of tau pathology and structural integrity but has only evaluated the influence of tau pathology without also additionally considering measures of Aβ.

In a population of cognitively normal and mildly impaired older adults, the current work examines the influence of Aβ and NFT pathology on structural integrity. We examine both the concurrent relationship between cortical thickness and pathology and the relationship between current levels of pathology and antecedent longitudinal change in cortical thickness. By considering both pathologies simultaneously, it is possible to estimate the unique influence each has on structural atrophy. This is critical not only to understand how tau pathology is related to another marker of neurodegeneration but also to explore whether tau pathology mediates prior observed relationships between Aβ and gray matter health.

2. Methods

2.1. Participants

Participants were selected from ongoing studies on aging and dementia from the Knight Alzheimer's Disease Research Center at Washington University. Cognitive status was assessed using the clinical dementia rating (CDR) [38]. Participants were required to have tau PET imaging and structural MRI at their most recent neuroimaging assessment. The cross-sectional cohort consisted of 178 individuals (age 46–91 years) with either no cognitive impairment (n = 156, CDR = 0) or very mild dementia (n = 22,

CDR = 0.5). From this initial population, 123 individuals had at least one MRI session that preceded the acquisition of tau PET (age 55–91 years; n = 111, CDR = 0; n = 12, CDR = 0.5). Full demographics for the cohort at the time of the tau PET session are presented in Table 1.

2.2. MRI acquisition and processing

T1-weighted images were acquired using a magnetization-prepared rapid gradient-echo sequence on a 3T Siemens scanner. Scans had a resolution of either $1 \times 1 \times 1.25$ mm or $1 \times 1 \times 1$ mm. Structural scans were processed with FreeSurfer [39]. For each hemisphere, cortical thickness values were obtained for all FreeSurfer cortical regions of interest (ROIs), and volumes were obtained for all FreeSurfer subcortical ROIs. Cortical thickness was calculated as the shortest distance between the cortical gray/white boundary and the gray/cerebrospinal fluid (CSF) boundary [40]. Cortical surface meshes are placed into a common anatomical space within FreeSurfer for vertex-wise analyses. Parcellations of the T1-weighted image into cortical and subcortical regions were also performed for utilization in the processing of PET data. Longitudinal data were processed through the FreeSurfer 5.3 longitudinal stream [41]. There were a total of 390 sessions in the longitudinal analyses (mean 3.1 visits, 5.7 years).

2.3. PET acquisition and processing

Aβ PET imaging was completed using [18F] AV-45 (florbetapir). Data from the 50- to 70-minute postinjection window were analyzed using an in-house pipeline using ROIs derived from FreeSurfer [39,42] (PET Unified Pipeline, https://github.com/ysu001/PUP). Tau PET imaging was performed using [18F] AV-1451 (flortaucipir). Data from the 80- to 100-minute postinjection window were analyzed. For both tracers, regional estimates were transformed into standardized uptake value ratios using a cerebellar cortex reference region, although alternate

Table 1
Sample demographics

Variable	Cross-sectional cohort (N = 178)	Longitudinal cohort (N = 123)
Age, years	70.1 (8.2)	70.8 (8.4)
Female (%)	106 (60)	74 (60)
MMSE	29.0 (1.8)	29.1 (1.9)
CDR-sum	0.3 (0.8)	0.2 (0.7)
AV-45 summary (SUVR)	1.27 (0.64)	1.29 (0.66)
AV-1451 summary (SUVR)	1.29 (0.35)	1.26 (0.30)
Months between AV-45 and AV-1451	3.6 (6.7)	4.3 (7.8)
Follow-up (years)		5.7 (2.4)
Follow-up (visits)		3.1 (1.1)

Abbreviations: CDR-sum, Clinical Dementia Rating–sum of boxes; MMSE, Mini–Mental Status Examination; SUVR, standardized uptake value ratio.
NOTE. Unless otherwise noted values represent means and standard deviations.

reference regions are also used in the literature [43]. Data were partial volume corrected using a regional spread function technique [44,45]. This approach corrects for the spillover signal from adjacent ROIs based upon the scanner point spread function and the relative distance between ROIs. ROI PET data were averaged across hemispheres for statistical analyses. A summary global Aβ [42] and tau [30] measures were calculated as previously published. On average, PET data were acquired within 3.6 months of one another.

2.4. Statistical analyses

Cross-sectional vertex-wise analyses were performed using the FreeSurfer Qdec application (www.surfer.nmr.mgh.harvard.edu). Three statistical models were examined using general linear models. The first related the summary measure of tau [30], as measured with flortaucipir, to vertex measures of cortical thickness. The second model related the Aβ summary measure, as measured with florbetapir, to vertex measurements of cortical thickness. Finally, to assess the unique influence of each pathology, the last model included both the Aβ and tau summary measures. All three models were run separately for the left and right hemispheres and included current age, gender, and scan resolution (1 × 1 × 1 or 1 × 1 × 1.25) as covariates. Vertices were considered significant after a false discovery rate correction considering both hemispheres.

Longitudinal analyses were performed two ways. The first set of analyses examined relationships of pathology with antecedent longitudinal change in cortical thickness at the cortical surface level using spatiotemporal linear mixed-effects (LMEs) models [14,46] implemented in MATLAB. LMEs are highly flexible approaches for analyzing longitudinal neuroimaging data because they can handle unequal numbers of data points and temporal spacing between assessments across subjects. The spatiotemporal approach is an extension of LMEs for mass-univariate analyses but also takes into account pooled covariance structure across neighboring vertices of homogenous regions. Three models were again run and were similar in structure to the cross-sectional models. In the first model, preceding longitudinal change in cortical thickness was predicted by the main effects of our current tau PET summary measure, gender, current age, time, scan resolution (1 × 1 × 1 or 1 × 1 × 1.25), and the interaction between tau PET and time. Models included random subject-specific slopes and intercepts. The second model implemented was identical in structure but used Aβ PET rather than tau as a predictor. The third, combined model examined the main effects and interactions with time of both global tau and Aβ PET. All three models were implemented separately for the left and right hemispheres, and vertices were considered significant after surviving false discovery rate correction accounting for comparisons in both hemispheres.

Finally, a series of LME data were run using ROIs derived from FreeSurfer to examine the effects of local pathology on local atrophy. Regional data were averaged between left and right hemispheres. Instead of examining the association between global summaries of Aβ and tau and cortical thickness, these analyses specifically modeled Aβ and tau PET binding within each ROI (e.g., precuneus) to thickness in that same ROI. This was done to avoid any bias that could be introduced by using summary measures formed from specific ROIs. The first model looked at the relationship between longitudinal measurements of thickness in that ROI predicted by main effects of current tau in that specific ROI, gender, current age, time, scan resolution, and the time by tau interaction. Models contained subject-specific random-effects intercepts and slopes. Similar models were run using Aβ rather than tau PET as a predictor, and finally combined models including both tau and Aβ and their interactions with time. These three models were run for all 34 cortical regions identified by FreeSurfer. Models were implemented using the lme4 package in R, version 3.4.1, and ROIs were considered significant after false discovery rate correction.

3. Results

3.1. Cross-sectional associations with global pathology

The vertex-wise results are presented in the left-hand column of Fig. 1. Fig. 1A depicts those vertices that had a significant relationship with the global tau PET measure. Fig. 1B depicts those vertices significantly related to the global Aβ PET measure. Fig. 1C shows those vertices significantly related to tau while additionally controlling for levels of Aβ. There were no vertices significantly related to Aβ when entered alone (Fig. 1B) or when tau was also included in the model (not shown). For simplicity, only the results from the left hemisphere are presented. Results for the right hemisphere are highly similar and presented in Supplementary Fig. 1.

3.2. Longitudinal associations with global pathology

Results from the spatiotemporal LMEs are presented in the right-hand column of Fig. 1. Fig. 1D shows those areas of the cortex that showed a significant global tau burden by time interaction, that is, how current levels of tau predict antecedent thickness change in cortical thickness. Fig. 1E depicts the Aβ by time interaction. Fig. 1F shows the tau by time interaction after additionally controlling for the main effect of global Aβ burden and Aβ by time interaction. There were no significant Aβ by time effects once tau was simultaneously considered in the model.

3.3. Longitudinal associations with local pathology

Results examining the relationships between antecedent structural change and local AD pathologies are
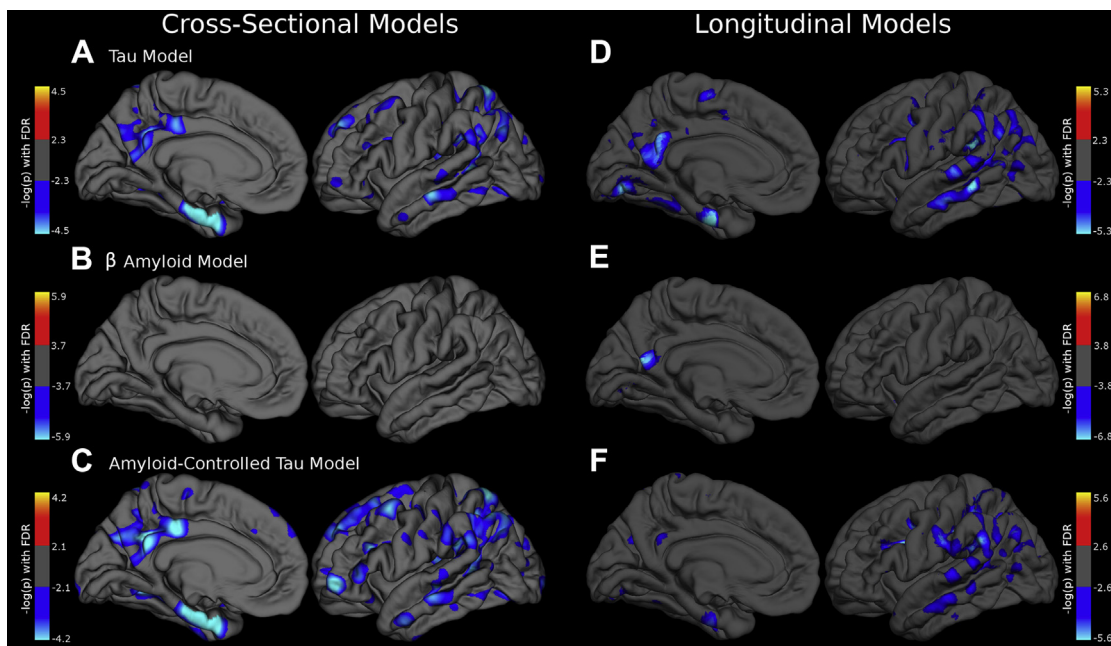
Fig. 1. The relationship between global AD pathology and gray matter. Three GLMs were implemented to estimate vertex-wise relationships between (A) global tau PET summary measure, (B) Aβ mean cortical SUVR, or (C) global tau controlling for Aβ, and left-hemisphere cross-sectional cortical thickness. Spatiotemporal LMEs models were used to investigate relationships between (D) global tau and time from initial MRI, (E) global Aβ and time, or (F) global tau and time controlling for Aβ and time, and antecedent longitudinal change in cortical thickness. All models controlled for the main effects of gender, current age, and scan resolution. Cross-sectional models used the Qdec multiple comparisons correction (FDR) procedure at $P < .025$ level to approximate comparisons in both hemispheres. Longitudinal models used the LME FDR2 comparisons correction in MATLAB and accounted for comparisons in both hemispheres. Values depicted from each model are thresholded at the level of significance identified by their respective FDR procedures. Abbreviations: Aβ, amyloid β; AD, Alzheimer's disease; FDR, false discovery rate; GLM, general linear model; LMEs, linear mixed-effects; MRI, magnetic resonance imaging; PET, positron emission tomography; SUVR, standardized uptake value ratio.

shown in Fig. 2 and presented in Table 2. To be visually consistent with Fig. 1, results are displayed on the left hemisphere but represented the statistical results from the average of data from left and right hemispheres. Fig. 2A depicts the significant regional tau burden by time interaction (e.g., the relationship between precuneus tau and change in precuneus cortical thickness). Fig. 2B depicts the local Aβ by time interaction. Fig. 2C depicts the local tau by time interaction when both tau and Aβ main effects and interactions were considered in the model simultaneously. There were no significant associations between local Aβ and change in cortical thickness once tau was additionally considered in the model.

4. Discussion

Prior work has demonstrated that structural MRI is a sensitive marker to AD dementia [1–5] and preclinical AD [4,5,8–10]. The advent of tau PET imaging has provided another *in vivo* biomarker of the molecular pathology in AD. The current work examined the association between cortical thickness and tau pathology measured with flortaucipir PET. We found that current levels of tau PET binding, rather than Aβ PET, were related to concurrent cortical thinning and preceding structural atrophy.

We found that both global and local levels of florbetapir were associated with greater antecedent atrophy. This is consistent with prior work in the field demonstrating structural declines in preclinical AD [4,5,8–10]. Early work has also indicated a significant relationship between tau PET binding and gray matter health [34–37]. When simultaneously considering both biomarkers, levels of tau PET mediated the effects of Aβ on cortical thickness. This suggests that in prior work, the association between gray matter and Aβ may have been a proxy for emerging NFT pathology. This also suggests that the relationship between tau PET and cortical thickness is distinct from the influence of Aβ.

The association between increasing levels of tau PET and cortical thinning was not restricted to the medial temporal lobe but was widespread throughout the temporal, occipital, parietal, and even portions of the frontal lobes. The effects in the temporal and parietal regions were particularly reminiscent of spatial signatures seen when examining whole-brain atrophy maps in AD [3–5], indicating a stable network of brain regions that also demonstrate tau-related atrophy. The pattern of areas demonstrating atrophy is also more similar to the spatial topography of tau rather than Aβ PET [22–28,31]. This effect was not however simply a product of the regions going into our summary measures. Analyses looking only at local tau and Aβ accumulation
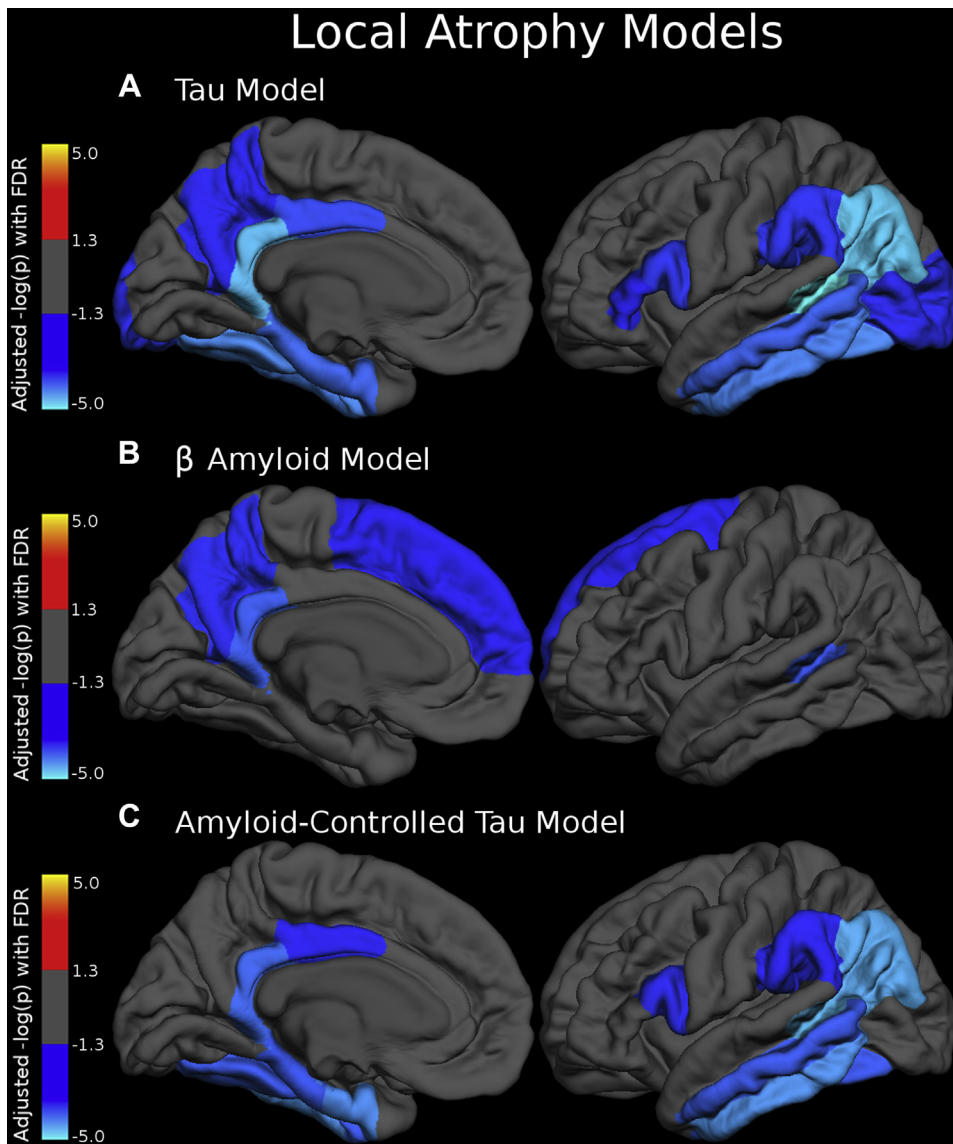
Fig. 2. The relationship between local AD pathology and gray matter. Linear mixed-effects models were implemented to model region-wise relationships between (A) local tau and time, (B) local Aβ and time, or (C) local tau and time controlling for local Aβ and time, on longitudinal local cortical thickness in all 34 FreeSurfer cortical regions. All models controlled for the main effects of gender, age, and scan resolution. Both hemispheres' values were averaged together. Values depicted are adjusted $-\log_{10}(P)$ values after FDR correction for multiple comparisons. Abbreviations: AD, Alzheimer's disease; FDR, false discovery rate.

recapitulated similar regional maps, suggesting a stronger local relationship between structural atrophy and tau than atrophy and Aβ.

The current work and prior results [35] indicate that NFT pathology measured with flortaucipir is related to cross-sectional cortical thinning, as well as atrophy that has occurred over the previous years. In models of AD patho-physiology [47], as well as work with autosomal-dominant AD [48], changes in tau pathology occur before structural changes seen with MRI. Such frameworks would suggest that tau pathology would be a stronger predictor of *future* rather than *retrospective* atrophy. Such a temporal relationship, for example, tau leading MRI with a time lag, could

still account for the current results. For example, we also found that rates of MRI change were also related to current levels of Aβ, although there is strong evidence that elevations in Aβ plaque deposition precedes all other pathologies [48]. Rates of structural atrophy may simply serve as a rough marker of the disease stage. As a result, greater antecedent atrophy could predict current Aβ or tau PET, even if that is not the correct causative temporal direction.

Alternatively, the temporal ordering of tau relative to structural MRI has been based on CSF total tau and phosphorylated tau. Although CSF and PET measures of tau are modestly correlated [23,29,37], these two markers likely measure distinct but related aspects of tau. Just as there appears to be

Table 2
Regional effects relating tau and Aβ to longitudinal rates of atrophy

Region	Aβ × time interaction			Tau × time interaction			Tau × time controlling for Aβ × time		
	B	t-value	Adjusted P value	B	t-value	Adjusted P value	B	t-value	Adjusted P value
Banks of the superior temporal sulcus	**−0.0039**	**−2.84**	**.00583**	**−0.0109**	**−5.15**	**.00000**	**−0.0109**	**−4.06**	**.00010**
Caudal anterior cingulate cortex	0.0004	0.2709	.78705	−0.0049	−0.85	.39591	−0.0052	−0.89	.37662
Caudal middle frontal gyrus	−0.0025	−1.6629	.10095	−0.0074	−1.51	.13530	−0.0044	−0.78	.43531
Cuneus	0.0002	0.0719	.94276	−0.0042	−0.67	.50606	−0.0042	−0.67	.50548
Entorhinal cortex	0.0008	0.0928	.92640	**−0.0209**	**−3.09**	**.00267**	**−0.0269**	**−3.61**	**.00054**
Frontal pole	−0.0006	−0.2986	.76560	0.0063	1.18	.24033	0.0069	1.26	.20816
Fusiform gyrus	−0.0038	−1.8799	.06381	**−0.0147**	**−3.55**	**.00060**	**−0.0147**	**−2.91**	**.00454**
Inferior parietal cortex	−0.0021	−1.8018	.07619	**−0.013**	**−4.18**	**.00005**	**−0.0147**	**−3.85**	**.00016**
Inferior temporal cortex	−0.001	−0.6511	.51701	**−0.0103**	**−3.43**	**.00085**	**−0.0132**	**−3.64**	**.00040**
Insula	−0.0039	−1.7147	.09024	−0.0035	−0.57	.56754	−0.0017	−0.27	.79159
Isthmus cingulate	**−0.0062**	**−2.9631**	**.00403**	**−0.0191**	**−4.02**	**.00009**	**−0.0158**	**−3.06**	**.00256**
Lateral occipital cortex	−0.0016	−0.9272	.35694	**−0.0078**	**−2.17**	**.03314**	−0.0084	−1.97	.05146
Lateral orbitofrontal cortex	−0.0014	−0.9398	.35083	−0.0009	−0.16	.87056	0.0004	0.08	.93691
Lingual gyrus	−0.0032	−1.1853	.23911	−0.0086	−1.39	.16707	−0.0079	−1.26	.21096
Medial orbital frontal cortex	−0.0027	−1.7311	.08784	−0.0123	−1.90	.06128	−0.0114	−1.76	.08258
Middle temporal gyrus	−0.0015	−1.0751	.28622	**−0.0096**	**−3.01**	**.00313**	**−0.0111**	**−2.90**	**.00434**
Paracentral gyrus	−0.0037	−1.4636	.14808	−0.0035	−0.49	.62762	−0.0019	−0.27	.79104
Parahippocampal cortex	−0.0047	−1.1655	.24740	**−0.02**	**−3.14**	**.00233**	**−0.0203**	**−2.86**	**.00519**
Pars opercularis	−0.0024	−1.5936	.11246	**−0.0138**	**−2.32**	**.02142**	**−0.0128**	**−2.13**	**.03453**
Pars orbitalis	0.0001	0.0628	.95017	0.006	1.25	.21444	0.0063	1.27	.20763
Pars triangularis	−0.0004	−0.3179	.75076	**−0.0099**	**−1.98**	**.04832**	−0.0096	−1.92	.05556
Pericalcarine cortex	−0.0003	−0.1267	.89929	0.0026	0.31	.75614	0.0027	0.32	.74731
Postcentral gyrus	0.0006	0.2626	.79360	−0.0014	−0.21	.83138	−0.0017	−0.26	.79910
Posterior cingulate cortex	−0.0024	−1.9147	.05899	**−0.0141**	**−2.67**	**.00874**	**−0.012**	**−2.05**	**.04273**
Precentral gyrus	−0.0029	−0.9078	.36737	−0.0087	−0.84	.40198	−0.0068	−0.64	.52336
Precuneus cortex	**−0.0024**	**−2.1989**	**.03179**	**−0.0098**	**−2.11**	**.03777**	**−0.0067**	**−1.30**	**.19534**
Rostral anterior cingulate cortex	−0.0001	−0.0734	.94167	0.0017	0.25	.80612	0.0017	0.25	.80556
Rostral middle frontal	−0.0008	−0.6686	.50571	−0.0026	−0.51	.60828	−0.0023	−0.45	.65569
Superior frontal cortex	−0.0024	−2.0056	.04637	−0.0059	−1.13	.26050	−0.0039	−0.74	.45983
Superior parietal cortex	−0.0002	−0.1315	.89578	−0.0022	−0.47	.63724	−0.0024	−0.44	.66145
Superior temporal gyrus	−0.0021	−1.2591	.21213	−0.0072	−1.49	.13919	−0.0058	−1.08	.28262
Supramarginal gyrus	−0.0014	−0.9435	.34642	**−0.0119**	**−2.30**	**.02254**	**−0.0115**	**−2.05**	**.04189**
Temporal pole	0.0001	0.0149	.98810	−0.0045	−0.50	.61688	−0.0055	−0.55	.58304
Transverse temporal gyrus	−0.0026	−0.8029	.42423	0.0052	0.58	.56118	0.0071	0.77	.44330

Abbreviation: Aβ, amyloid β.
NOTE. Bold values represent multiple comparison adjusted P values <.05.

a temporal lag between CSF and PET measures of Aβ [49,50], there is likely a temporal delay between changes in CSF and PET measures of tau. As a result, tau PET may be later in disease progression and more proximal or even later to changes seen with structural MRI. Neuronal dysfunction and reduced dendritic branching may initially occur and manifest on MRI before mature tangles [20] that are bound by flortaucipir form. Prospective acquisition of both longitudinal MRI and tau PET along with work in autosomal-dominant AD populations will help to clarify the temporal dynamics of tau PET relative to other markers.

Acknowledgments

Supplementary data

Supplementary data related to this article can be found at https://doi.org/10.1016/j.dadm.2018.02.003.

RESEARCH IN CONTEXT

1. Systematic review: The authors reviewed the literature using traditional sources (e.g. PubMed and Google Scholar) for articles examining structural decline in preclinical and clinical Alzheimer's disease as well as for work using tau positron emission tomography imaging. Although tau positron emission tomography imaging has been related to neurodegenerative biomarkers, it is still not understood how tau pathology relates to cortical atrophy in relation to amyloid β deposition.

2. Interpretation: Our work found that tau rather than amyloid β predicts concurrent and antecedent gray matter loss. This result is consistent with neuropathology work indicating that tau pathology is a better marker of cognitive impairment than amyloid β.

3. Future directions: The manuscript found relationships between preceding changes in cortical integrity and current levels of tau pathology. Future work using longitudinal measures of both tau and magnetic resonance imaging and will help to further clarify the temporal dynamic between these markers.

References

[1] Scheltens P, Leys D, Barkhof F, Huglo D, Weinstein HC, Vermersch P, et al. Atrophy of medial temporal lobes on MRI in "probable" Alzheimer's disease and normal ageing: diagnostic value and neuropsychological correlates. J Neurol Neurosurg Psychiatry 1992;55:967–72.

[2] Jack CR, Petersen RC, Xu CY, Waring SC, Brien PCO, Tangalos EG, et al. Medial temporal atrophy on MRI in normal aging and very mild Alzheimer's disease. Neurology 1997;49:786–94.

[3] Baron JC, Chételat G, Desgranges B, Perchey G, Landeau B, de la Sayette V, et al. In vivo mapping of gray matter loss with voxel-based morphometry in mild Alzheimer's disease. Neuroimage 2001; 14:298–309.

[4] Dickerson BC, Bakkour A, Salat DH, Feczko E, Pacheco J, Greve DN, et al. The cortical signature of Alzheimer's disease: regionally specific cortical thinning relates to symptom severity in very mild to mild AD dementia and is detectable in asymptomatic amyloid-positive individuals. Cereb Cortex 2009;19:497–510.

[5] Sabuncu MR, Desikan RS, Sepulcre J, Yeo BTT, Liu H, Schmansky NJ, et al. The dynamics of cortical and hippocampal atrophy in Alzheimer disease. Arch Neurol 2011;68:1040–8.

[6] Karas GB, Scheltens P, Rombouts SA, Visser PJ, Van Schijndel RA, Fox NC, et al. Global and local gray matter loss in mild cognitive impairment and Alzheimer's disease. Neuroimage 2004;23:708–16.

[7] Schultz SA, Oh JM, Koscik RL, Dowling NM, Gallagher CL, Carlsson CM, et al. Subjective memory complaints, cortical thinning, and cognitive dysfunction in middle-age adults at risk of AD. Alzheimers Dement 2015;1:33–40.

[8] Gordon BA, Blazey T, Su Y, Fagan AM, Holtzman DM, Morris JC, et al. Longitudinal β-Amyloid deposition and hippocampal volume in preclinical Alzheimer disease and suspected non–Alzheimer disease pathophysiology. JAMA Neurol 2016;73:1192–200.

[9] Wang L, Benzinger TL, Hassenstab J, Blazey T, Owen C, Liu J, et al. Spatially distinct atrophy is linked to β-amyloid and tau in preclinical Alzheimer disease. Neurology 2015;84:1254–60.

[10] Chételat G, Villemagne VL, Villain N, Jones G, Ellis KA, Ames D, et al. Accelerated cortical atrophy in cognitively normal elderly with high β-amyloid deposition. Neurology 2012;78:477–84.

[11] Devanand DP, Pradhaban G, Liu X, Khandji A, De Santi S, Segal S, et al. Hippocampal and entorhinal atrophy in mild cognitive impairment: prediction of Alzheimer disease. Neurology 2007; 68:828–36.

[12] Apostolova LG, Dutton RA, Dinov ID, Hayashi KM, Toga AW, Cummings JL, et al. Conversion of mild cognitive impairment to Alzheimer disease predicted by hippocampal atrophy maps. Arch Neurol 2006;63:693–9.

[13] Bakkour A, Morris JC, Dickerson BC. The cortical signature of prodromal AD: regional thinning predicts mild AD dementia. Neurology 2009;72:1048–55.

[14] Bernal-Rusiel JL, Reuter M, Greve DN, Fischl B, Sabuncu MR. Spatiotemporal linear mixed effects modeling for the mass-univariate analysis of longitudinal neuroimage data. Neuroimage 2013;81:358–70.

[15] Dickerson BC, Stoub TR, Shah RC, Sperling R a, Killiany RJ, Albert MS, et al. Alzheimer-signature MRI biomarker predicts AD dementia in cognitively normal adults. Neurology 2011; 76:1395–402.

[16] Chételat G, Villemagne VL, Bourgeat P, Pike KE, Jones G, Ames D, et al. Relationship between atrophy and beta-amyloid deposition in Alzheimer disease. Ann Neurol 2010;67:317–24.

[17] Archer HA, Edison P, Brooks DJ, Barnes J, Frost C, Yeatman T, et al. Amyloid load and cerebral atrophy in Alzheimers disease: An [11] C-PIB positron emission tomography study. Ann Neurol 2006;60:145–7.

[18] Chien DT, Bahri S, Szardenings AK, Walsh JC, Mu F, Su MY, et al. Early clinical PET imaging results with the novel PHF-Tau Radioligand [F-18]-T807. J Alzheimers Dis 2013;34:457–68.

[19] Marquie M, Normandin MD, Vanderburg CR, Costantino I, Bien EA, Rycyna LG, et al. Validating novel tau PET tracer [F-18]-AV-1451 (T807) on postmortem brain tissue. Ann Neurol 2015;78:787–800.

[20] Lowe VJ, Curran G, Fang P, Liesinger AM, Josephs KA, Parisi JE, et al. An autoradiographic evaluation of AV-1451 Tau PET in dementia. Acta Neuropathol Commun 2016;4:58.

[21] Xia C-F, Arteaga J, Chen G, Gangadharmath U, Gomez LF, Kasi D, et al. [18F]T807, a novel tau positron emission tomography imaging agent for Alzheimer's disease. Alzheimers Dement 2013;9:666–76.

[22] Brier MR, Gordon B, Friedrichsen K, McCarthy J, Stern A, Christensen J, et al. Tau and Aβ imaging, CSF measures, and cognition in Alzheimer's disease. Sci Transl Med 2016;8:338ra66.

[23] Gordon BA, Friedrichsen K, Brier M, Blazey T, Su Y, Christensen J, et al. The relationship between cerebrospinal fluid markers of Alzheimer pathology and positron emission tomography tau imaging. Brain 2016;139:2249–60.

[24] Johnson KA, Schultz A, Betensky RA, Becker JA, Sepulcre J, Rentz D, et al. Tau PET imaging in aging and early Alzheimer's disease. Ann Neurol 2016;79:110–9.

[25] Schöll M, Lockhart SN, Schonhaut DR, Schwimmer HD, Rabinovici GD, Correspondence WJ, et al. PET imaging of tau deposition in the aging human brain. Neuron 2016;89:971–82.

[26] Cho H, Choi JY, Hwang MS, Lee JH, Kim YJ, Lee HM, et al. Tau PET in Alzheimer disease and mild cognitive impairment. Neurology 2016; 87:375–83.

[27] Day GS, Gordon BA, Jackson K, Christensen JJ, Rosana Ponisio M, Su Y, et al. Tau-PET binding distinguishes patients with early-stage posterior cortical atrophy from amnestic Alzheimer disease dementia. Alzheimer Dis Assoc Disord 2017;31:87–93.

[28] Schwarz AJ, Yu P, Miller BB, Shcherbinin S, Dickson J, Navitsky M, et al. Regional profiles of the candidate tau PET ligant 18F-AV-1451 recapitulate key features of Braak histopathological stages. Brain 2016;139:1539–50.

[29] Chhatwal JP, Schultz AP, Marshall GA, Boot B, Gomez-Isla T, Dumurgier J, et al. Temporal T807 binding correlates with CSF tau and phospho-tau in normal elderly. Neurology 2016;87:920–6.

[30] Mishra S, Gordon BA, Su Y, Christensen J, Friedrichsen K, Jackson K, et al. AV-1451 PET imaging of tau pathology in preclinical Alzheimer disease: defining a summary measure. Neuroimage 2017;161:171–8.

[31] Bischof GN, Jessen F, Fliessbach K, Dronse J, Hammes J, Neumaier B, et al. Impact of tau and amyloid burden on glucose metabolism in Alzheimer's disease. Ann Clin Transl Neurol 2016;3:934–9.

[32] Ossenkoppele R, Schonhaut DR, Schöll M, Lockhart SN, Ayakta N, Baker SL, et al. Tau PET patterns mirror clinical and neuroanatomical variability in Alzheimer's disease. Brain 2016;139:1551–67.

[33] Smith R, Wibom M, Olsson T, Hägerström D, Jögi J, Rabinovici GD, et al. Posterior accumulation of tau and concordant hypometabolism in an early-onset Alzheimer's disease patient with presenilin-1 mutation. J Alzheimers Dis 2016;51:339–43.

[34] Wang L, Benzinger TL, Su Y, Christensen J, Friedrichsen K, Aldea P, et al. Evaluation of tau imaging in staging Alzheimer disease and revealing interactions between β-Amyloid and tauopathy. JAMA Neurol 2016;73:1070.

[35] LaPoint MR, Chhatwal JP, Sepulcre J, Johnson KA, Sperling RA, Schultz AP. The association between tau PET and retrospective cortical thinning in clinically normal elderly. Neuroimage 2017;157:612–22.

[36] Xia C, Makaretz SJ, Caso C, McGinnis S, Gomperts SN, Sepulcre J, et al. Association of in vivo [18F]AV-1451 tau PET imaging results with cortical atrophy and symptoms in typical and atypical Alzheimer disease. JAMA Neurol 2017;74:427.

[37] Mattsson N, Schöll M, Strandberg O, Smith R, Palmqvist S, Insel PS, et al. (18)F-AV-1451 and CSF T-tau and P-tau as biomarkers in Alzheimer's disease. EMBO Mol Med 2017;9:1212–23.

[38] Morris JC. The Clinical Dementia Rating (CDR): current version and scoring rules. Neurology 1993;43:2412–4.

[39] Fischl B. FreeSurfer. Neuroimage 2012;62:774–81.

[40] Fischl B, Dale AMM. Measuring the thickness of the human cerebral cortex from magnetic resonance images. Proc Natl Acad Sci U S A 2000;97:11050–5.

[41] Reuter M, Schmansky NJ, Rosas HD, Fischl B. Within-subject template estimation for unbiased longitudinal image analysis. Neuroimage 2012;61:1402–18.

[42] Su Y, D'Angelo GM, Vlassenko AG, Zhou G, Snyder AZ, Marcus DS, et al. Quantitative Analysis of PiB-PET with FreeSurfer ROIs. PLoS One 2013;8:e73377.

[43] Brendel M, Högenauer M, Delker A, Sauerbeck J, Bartenstein P, Seibyl J, et al. Improved longitudinal [18F]-AV45 amyloid PET by white matter reference and VOI-based partial volume effect correction. Neuroimage 2015;108:450–9.

[44] Su Y, Blazey TM, Snyder AZ, Raichle ME, Hornbeck RC, Aldea P, et al. Quantitative Amyloid imaging using image-derived arterial input function. PLoS One 2015;10:e0122920.

[45] Rousset OG, Ma Y, Evans AC. Correction for partial volume effects in PET: Principle and validation. J Nucl Med 1998;39:904–11.

[46] Bernal-Rusiel JL, Greve DN, Reuter M, Fischl B, Sabuncu MR, for the Alzheimer's Disease Neuroimaging I. Statistical analysis of longitudinal neuroimage data with Linear Mixed Effects models. Neuroimage 2012;66C:249–60.

[47] Jack CR, Knopman DS, Jagust WJ, Petersen RC, Weiner MW, Aisen PS, et al. Tracking pathophysiological processes in Alzheimer's disease: an updated hypothetical model of dynamic biomarkers. Lancet Neurol 2013;12:207–16.

[48] Bateman RJ, Xiong C, Benzinger TLS, Fagan AM, Goate A, Fox NC, et al. Clinical and biomarker changes in dominantly inherited Alzheimer's disease. N Engl J Med 2012;367:795–804.

[49] Vlassenko AG, McCue L, Jasielec MS, Su Y, Gordon BA, Xiong C, et al. Imaging and cerebrospinal fluid biomarkers in early preclinical Alzheimer disease. Ann Neurol 2016;80:379–87.

[50] Palmqvist S, Mattsson N, Hansson O, Alzheimer's Disease Neuroimaging Initiative. Cerebrospinal fluid analysis detects cerebral amyloid-β accumulation earlier than positron emission tomography. Brain 2016;139:1226–36.